Continuous Time Random Walk Analysis of Solute Transport in Fractured Porous Media

Andrea Cortis and Jens Birkholzer

Lawrence Berkeley National Laboratory

Abstract

The objective of this work is to discuss solute transport phenomena in fractured porous media, where the macroscopic transport of contaminants in the highly permeable inter-connected fractures can be strongly affected by solute exchange with the porous rock matrix. We are interested in a wide range of rock types, with matrix hydraulic conductivities varying from almost impermeable (e.g., granites) to somewhat permeable (e.g., porous sandstones). In the first case, molecular diffusion is the only transport process causing the transfer of contaminants between the fractures and the matrix blocks. In the second case, additional solute transfer occurs as a result of a combination of advective and dispersive transport mechanisms, with considerable impact on the macroscopic transport behavior. We start our study by conducting numerical tracer experiments employing a discrete (microscopic) representation of fractures and matrix. Using the discrete simulations as a surrogate for the "correct" transport behavior, we then evaluate the accuracy of macroscopic (continuum) approaches in comparison with the discrete results. However, instead of using dual-continuum models, which are quite often

used to account for this type of heterogeneity, we develop a macroscopic model based on the Continuous Time Random Walk (CTRW) framework, which characterizes the interaction between the fractured and porous rock domains by using a probability distribution function of residence times. A parametric study of how CTRW parameters evolve is presented, describing transport as a function of the hydraulic conductivity ratio between fractured and porous domains.

Introduction

The internal heterogeneity of fractured porous formations is a significant obstacle to the prediction of solute transport processes (Berkowitz, 2002). The macroscopic transport of contaminants in such systems is mainly carried out in high-permeable, interconnected fractures, but most of the capacity for storing a pollutant is provided by the low-permeability porous matrix. Because of the much slower transport in the matrix, steep concentration gradients may occur between the fractures and the porous blocks, giving rise to a local disequilibrium. The terms “macroscopic” and “local” or “microscopic” are used in this paper to define different scales of interest. The macroscopic scale incorporates a large number of individual fractures and matrix blocks, e.g., between a contaminant source and a monitoring well. In contrast, the local (microscopic) scale is on the order of single fractures and single matrix blocks. The local disequilibrium situation with regard to the solute concentrations in fractures and matrix can lead to significant solute transfer at the fracture/matrix interfaces. This local transfer can strongly influence the macroscopic solute transport in a fractured porous formation, and thus needs to be accounted for in numerical models (Berkowitz, 2002).

Generally, the numerical simulation of flow and transport processes in fractured porous media can be performed with discrete models or continuum models (e.g., Berkowitz, 2002; Neuman, 2005). Discrete models describe the spatial structure of the fracture-matrix system in great detail on a microscopic level, and thus allow for a more accurate simulation than continuum models. However, since discrete models are limited in their applicability to field problems, upscaling methods are commonly employed to develop macroscopic models, simulating the flow and solute transport behavior in sufficiently large computational cells and assigning suitably averaged "effective" properties to them. In fractured porous formations, where the local disequilibrium between fractures and matrix cannot be neglected, researchers have often applied so-called dual-continuum models (Barenblatt et al., 1960). Here, the heterogeneous formation is separated into two superimposed, interacting media, one representing the fracture system with high conductivity, the other representing the porous rock matrix with high storage capacity. Because both media are treated as different systems, the flow and transport processes are described by two separate sets of equations coupled by transfer terms to account for the exchange of mass at the common boundary.

Despite the simplification with regard to neglecting microscopic transport processes, numerical modeling of dual-continuum systems is still a complicated process. For example, different types of dual-continuum approaches are needed depending on the hydrologic characteristics of the porous matrix. In the general form of a dual-continuum model, the regional flow and transport processes take place in both domains. In many

71 formations, however, the regional flow and transport processes in the matrix continuum
72 can be neglected because the hydraulic conductivity of the matrix is almost negligible
73 compared to that of the fracture continuum, such as in crystalline rocks or shale (Bodin et
74 al., 2003). In such cases, the matrix continuum acts as a local storage domain for the
75 regional flow and transport in the fracture continuum. The governing equation for the
76 matrix continuum can then be simplified by eliminating the macroscopic flow and
77 transport terms so that only the local fluid flow or solute exchange with the fracture
78 continuum needs to be considered. In the first general form of a dual-continuum model,
79 we use the term "dual-permeability" (or mobile-mobile) model; the latter case is referred
80 to as a "dual-porosity" (or mobile-immobile) model (Simunek et al., 2003). Note that in a
81 dual-porosity model, the local fluid flow between fracture and matrix continua may be
82 neglected, e.g., when the flow field is steady-state as assumed in this paper (i.e., no local
83 pressure gradient between fractures and matrix) or when the matrix permeability is
84 sufficiently small. Matrix diffusion is then the only relevant solute transfer process at the
85 fracture-matrix interfaces.
86
87 A variety of dual-porosity (mobile-immobile) approaches have been described in the
88 literature, most of which with a focus on solute transport in fractured porous media.
89 Respective models have been developed with simple first-order transfer terms (e.g.,
90 Huyakorn et al., 1983a; Birkholzer and Rouve, 1994) or more complex higher-order
91 approaches, where local-scale detailed descriptions of diffusive transport are employed in
92 the immobile domain (e.g., Bibby, 1981; Huyakorn, 1983b, 1983c; Dykhuizen, 1990;
93 Zimmerman et al., 1990, 1993; Birkholzer and Rouve, 1994). Note that variations of

94 dual-porosity approaches have also been used to study solute-transport problems in
95 heterogeneous porous media bimodal permeability structures (e.g., Roth and Jury, 1993;
96 Haggerty and Gorelick, 1995; Feeley et al., 2000; Flach et al., 2004).
97
98 Macroscopic modeling of solute transport in dual-permeability (mobile-mobile) systems
99 is conceptually more challenging than in dual-porosity (mobile-immobile) systems. First,
100 the macroscopic transport processes need to be solved for in both continua, which
101 requires determination of hydrologic properties separately for the fractured and the
102 porous domain (e.g., Teutsch, 1988; Gerke and van Genuchten, 1993a). Furthermore, the
103 solute-transfer term needs to take into account not only diffusive transport, but also the
104 additional effects of advection and dispersion. Figure 1 schematically illustrates the
105 advective mass exchange between fractures and porous matrix, as solutes migrate within
106 matrix pores (driven by a regional gradient) and encounter flow in transverse fractures.
107 Birkholzer and Rouve (1994) proposed a dual-permeability approach with a specific
108 solute transfer term for such advective-dispersive mixing processes. In this approach, a
109 first-order exchange term is determined, based on the macroscopic flow in the matrix
110 continuum and the geometric characteristics of the fracture network. For dual-
111 permeability modeling of heterogeneous soils with high- and low-permeability regions,
112 Ahmadi et al. (1998), Cherblanc et al. (2003), and Cherblanc et al. (2007) developed a
113 volume averaging technique that allows definition of first-order transfer terms for
114 diffusive, dispersive, and advective processes.
115

As is apparent from the above discussion, dual-continuum models of various types are available for simulating solute transport in fractured porous media. However, while dual-porosity models have quite often been applied to field problems, dual-permeability applications have been less frequent. One of the crucial problems encountered when using dual-permeability models is the determination of the large-scale effective properties, which include the macroscopic flow and transport properties of the two domains, as well as the properties determining solute transfer between the two domains. This is not a trivial task. For example, while *a priori* estimates of solute transfer coefficients have been proposed for idealized subsurface geometries (e.g., Dykhuizen, 1990; Zimmerman et al., 1990, 1993; Gerke and van Genuchten, 1993b; Gwo et al., 1998 [for diffusive matrix transport]; Birkholzer and Rouve, 1994 [for advective matrix transport]), they are generally derived from calibration to field measurements. Furthermore, the *a priori* decision about the appropriate model to be used in a specific field situation—dual-porosity or dual-permeability—can be difficult, depending on the time and length scale of interest as well as the domain properties.

In this paper, we evaluate the applicability of the Continuous Time Random Walk (CTRW) theory for modeling solute transport in fractured porous formations, as an alternative to the traditional dual-continuum approach. The CTRW theory has been developed to explain and model anomalous, i.e., non-Fickian, transport in heterogeneous physical systems (Scher and Lax, 1973). Any deviation from perfect homogeneity induces retardation and/or acceleration of the solute, which cannot be represented by models based on the classical hypothesis of homogeneous transport. CTRW is an

139 effective upscaled method that treats unresolved (small-scale) heterogeneities
140 stochastically and resolved (large-scale) heterogeneities deterministically. CTRW has
141 found many useful applications in hydrogeological problems, including transport of
142 tracers in porous media (Bijecjic and Blunt, 2006), fracture networks (Berkowitz and
143 Scher, 1995, Noetinger et al., 2001a,b, Landereau et al., 2001), sandstones, sand columns,
144 unsaturated soils (Cortis and Berkowitz, 2004), karstic systems (Anwar et al., 2007), the
145 hyporheic zone (Boano et al., 2007), transient flow in highly heterogeneous permeable
146 systems (Cortis and Knudby, 2006), flow of emulsions in porous media (Cortis and
147 Ghezzehei, 2007), heat transfer in porous media (Emmanuel and Berkowitz, 2006), and
148 transport of biocolloids (Cortis et al., 2006).
149
150 Dentz and Berkowitz (2003) demonstrated that the CTRW method is formally equivalent
151 to the linear multirate mass-transfer (MRMT) concept (e.g., Haggerty and Gorelick,
152 1995). The dual-porosity approach is essentially a MRMT model with a specific mass-
153 transfer model accounting for heterogeneity in the solute exchange between mobile and
154 immobile regions. Our study aims at demonstrating that the CTRW framework not only
155 can substitute for dual-continuum approaches, but is generally applicable to fractured
156 porous formations over a wide range of matrix permeabilities. We do this by first
157 conducting numerical tracer experiments in discrete fracture-matrix systems (Berkowitz
158 et al., 1988, Birkholzer et al. 1993a,b, Birkholzer and Rouve, 1994, Rubin et al., 1996).
159 These simulations are assumed to represent the “correct” system behavior. In a second
160 step, the results of the discrete simulations are compared with the results from a
161 nonparametric best-fit solution of the CTRW method (Cortis, 2007).

2 Discrete Numerical Experiments

2.1 Methodology

Numerical tracer experiments are conducted using a discrete representation of individual fractures and matrix blocks, respectively. Because the flow and transport processes are simulated in great detail on a microscopic ("local") scale, we may assume that the discrete simulation results faithfully represent the transport corresponding to a given set of hydrologic properties, so that the results obtained using the CTRW method can be compared to these "correct" results.

Since our main interest here is phenomena related to fracture/matrix interaction and their impact on macroscopic solute transport, it is reasonable to restrict the discrete simulations to fractured formations with regular geometry and uniform properties. The randomness and heterogeneity of natural fracture networks would (1) create difficulties in interpreting the simulation results with regard to the purpose of our study, and (2) involve the difficult task of assigning effective continuum parameters. Issues of computational efficiency are to be considered as well, since the discrete simulation results need to be compared to continuum results on a sufficiently large scale.

Figure 2 illustrates the setup for the numerical experiments. An idealized formation is considered, with two orthogonal sets of parallel equidistant fractures embedded in porous permeable matrix blocks (Berkowitz et al., 1988; Birkholzer and Rouve, 1994; Lagendijk, 2005). A constant (steady-state) hydraulic gradient of 0.01 in the positive x-direction is imposed by prescribing appropriate hydraulic head boundary conditions at the inflow and

outflow cross sections of the model area. On the local scale, flow in the matrix follows the direction of the gradient, whereas flow in the fractures follows the fracture axis. On the macroscopic scale, however, both types of flow follow the positive x-direction, owing to the symmetry of the fracture network. We simulate the migration of an ideal tracer disposed uniformly along the inflow cross section, given by a relative concentration value of one imposed at the inflow boundary of the model area. The solute migrates through the model area in both the fractures and the porous permeable blocks; however, the transport in the fractures is several orders of magnitude faster. Initially, the model area is not contaminated.

Although the conceptual setup is highly idealized, it is consistent with the requirements needed for the present study. First, it represents the tortuous flow paths through a natural fracture network, providing a large interface for mixing between the fractures and the porous blocks. Second, the flow and transport processes in the domain are symmetrical to the x-axis, without any transverse dispersion stemming from the randomness and heterogeneity of the fracture network. It is therefore possible to use the system's symmetry and simulate only the long, thin sub domain depicted in the bottom of Figure 2, with the upper and lower boundaries representing no-flow boundaries. As indicated in the figure, the term "sector" refers to part of the model domain extending between two adjacent fracture intersections. We consider model domains consisting of a hundred, 0.5 m long, sectors, so that the total length of the model domain is 50 m in the x–direction, and 0.5 m in the y–direction.

207 The discrete simulation runs were performed with the standard GALERKIN-Finite-
208 Element-Code STRAFE6 using a Crank-Nicholson time weighting scheme (Lagendijk,
209 2005). Due to the heterogeneity of the formation, a refined discretization in space and
210 time was needed to meet the Peclet and Courant criteria. Triangle elements were used for
211 the porous matrix and one-dimensional line-elements for the fracture representation (see
212 example for two sectors in Figure 2, bottom). A total number of with 1,000 line elements
213 and 20,000 triangles was utilized, and simulation runs comprised up to 30,000 time steps.
214
215 Tables 1 and 2 summarize the geometrical and hydrological properties chosen for the
216 discrete simulations. These properties are similar to those used in the discrete numerical
217 experiments described in Birkholzer and Rouve (1994) and Lagendijk (2005). The
218 majority of them are kept constant in our study (Table 1), except for the hydraulic
219 conductivity in the matrix, which is varied in four sensitivity cases (Table 2). We expect
220 matrix conductivity to be the most important parameter defining (1) whether the fractured
221 porous formation is a mobile-immobile or a mobile-mobile system, and (2) whether the
222 solute exchange between fractures and matrix is dominated by diffusive or advective
223 processes. All values chosen represent reasonable parameters mentioned in the literature
224 as typical for actual field situations. Notice that the relevant fracture properties in Table 1
225 are given for single fractures, as represented in the discrete modeling exercise, but have
226 also been converted into fracture continuum parameters, as required in macroscopic
227 continuum approaches (fracture continuum conductivity and fracture continuum porosity).
228

229 Table 2 discusses the basic features of the four sensitivity cases. In Case 1, we consider a
230 small hydraulic conductivity in the matrix of 8.3×10^{-6} m/d; i.e., the porous matrix is
231 essentially impermeable. Cases 2 and 3 denote intermediate cases with conductivities of
232 2.0×10^{-3} m/d and 8.3×10^{-3} m/d, respectively, while Case 4 features a relatively high
233 matrix conductivity of 9.94×10^{-2} m/d. Notice the strong internal heterogeneity reflected
234 in the ratios of fracture to matrix continuum conductivity and transport velocity. With
235 respect to conductivity, these ratios range from 12,000 (Case 1) to 1 (Case 4); i.e., in the
236 latter case, the same magnitude of flow occurs in the two continua. With respect to
237 transport velocity, these ratios range from almost infinite (Case 1) to 250 (Case 4); i.e., in
238 all cases, the transport velocity in single fractures is much higher than the transport
239 velocity in the matrix. As discussed in Birkholzer and Rouve (1994), the internal
240 heterogeneity causes a solute-transport behavior in which the fast flow and transport in
241 the fractures is affected by more or less intense solute exchange with the matrix. In the
242 first case, with near-zero matrix permeability, molecular diffusion is the only transport
243 process causing the transfer of solutes between the fractures and the matrix blocks. In the
244 other cases, with increasing matrix conductivity, more and more solute mixing occurs
245 between fractures and the matrix, as a result of advective flow in the matrix, which has a
246 sizable impact on overall transport behavior (see Section 2.2).
247

248 **2.2 Simulation Results**

249 We shall first discuss simulation results on a local scale—i.e., on the scale of single
250 fractures and matrix blocks—to evaluate the basic phenomena of solute transport in
251 fracture-matrix systems. In Figure 3, we present the solute isoconcentration contours for

252 the discrete matrix blocks located in Sectors 3 and 4 of the model area. These sectors are
253 close enough to the contaminant source to feature a fast response, and yet far enough
254 away from it to be essentially unaffected by the inlet boundary condition. We then
255 discuss the macroscopic transport in the discrete fracture-matrix systems using
256 breakthrough curves (BTC, see Figure 4) obtained at selected locations along the model
257 domain (i.e., at 1 m, 5 m, 15 m, and 45 m from the inflow boundary, which corresponds
258 to 2, 10, 30, and 90 model sectors). The BTCs at these locations will be used to evaluate
259 the performance of the CTRW method.
260
261 Figure 3(a) depicts the discrete simulation results in Sectors 3 and 4 for Case 1, which
262 has an almost impermeable porous matrix. We notice a strong contaminant buildup near
263 the fractures, demonstrating that solutes migrate very fast in the fracture network. During
264 this fast advective transport, a small fraction of the solute migrates from the fractures into
265 the porous matrix. This process is slow: at 100 days, the major fraction of the matrix
266 blocks is not yet contaminated. The BTCs for Case 1 in Figure 4(a) exhibit the typical
267 transport behavior of dual-porosity (mobile-immobile) media. The tracer breakthrough
268 values initially increase very quickly, because of the large velocities in the fracture
269 network. The smaller the distance between observation point and tracer inlet, the more
270 significant the initial concentration buildup. Long tailing is observed after the initial
271 buildup, a result of the slow diffusive transfer between the fractures and the matrix pore
272 system. The dashed BTC indicates the local concentration differences between fractures
273 and matrix for a migration distance of 30 sectors. It is obvious that the formation would

need a very long time to equilibrate: significant local concentration differences can still be observed at 3,000 days.

Concentration contours for Cases 2 and 3 are presented in Figures 3(b) and 3(c), respectively, after 100 days of solute disposal. While the transport velocity in the fractures is still orders of magnitude higher than in the matrix (Table 2), the impact of increasing matrix permeability shows in the microscopic transport behavior. The asymmetrical concentration contours are a result of advective-dispersive transport in the matrix, acting in the positive x–direction. The diffusive transfer from the fractures into the matrix is complemented by this advective-dispersive component—thus, the faster concentration buildup in the matrix compared to Case 1. The effect of enhanced mixing between fractures and matrix also shows in the BTCs in Figures 4(b) and 4(c), where, compared to Case 1, equilibrium conditions are reached earlier and less tailing can be observed.

Case 4 presented in Figures 3(d) and 4(d) features a conductivity ratio of one between the fracture and matrix continua; i.e., 50% of the macroscopic flow is performed in the fractures and 50% in the matrix. The advective-dispersive mixing between the fracture and the matrix flow is so intense that the local concentrations equilibrate very fast, despite the still significant velocity-difference ratio of 250 between the two media. We present concentration contours at 20 days because the matrix blocks in Sectors 3 and 4 are completely contaminated after less than 100 days. (With a transport velocity of about 0.02 m/d in the matrix, a particle needs about 50 days to migrate along the two sectors, as

297 shown in Figure 3(d).) The breakthrough curves in Figure 4(d) resemble those of
298 advective-dispersive transport in a homogeneous medium; it seems that an almost
299 continuous front is moving through the formation.
300

301 # 3 CTRW Modeling of the Fractured-Rock Transport Problem

302 ## 3.1 Physical Motivation and Model Formulation

303 The CTRW framework is a generalization of the classical Random Walk (RW) method
304 so often used in the hydrogeological literature to solve the advection-dispersion equation
305 (ADE) of a passive tracer in a porous domain. In the RW approach, tracer density is
306 obtained by following the evolution of an ensemble of random walkers taking
307 (uncorrelated) jumps of constant length at random (uniform) direction in the unit time.
308 CTRW generalizes this physical picture by allowing the walker to jump according to a
309 probabilistic distribution function (pdf), $\Psi(x,\tau)$, of the length of a jump, x, and the
310 retention time, τ, at a given location, while keeping a uniform random distribution for the
311 jump direction. Assuming that the probability of the length of the jumps and the retention
312 time probability are statistically independent, we write $\Psi(x,\tau) = p(x)\psi(\tau)$, where p(x) is
313 the probabilistic distribution of the particle jump lengths, and $\psi(\tau)$ is the retention times
314 pdf. A detailed analysis of this uncoupling assumption can be found in Berkowitz et al.
315 (2006]. When both the p(x) and $\psi(\tau)$ pdfs have finite first and second moments, (e.g.,
316 uniform, decaying exponential), the CTRW and RW physical pictures can be considered
317 to be equivalent. If, however, either of the two has infinite variance (e.g., Cauchy, power-
318 law) than the CTRW yields qualitatively different physical pictures, and the random
319 paths are referred to as Levy walks and Levy flights, for the cases of infinite variance of

320 $\psi(\tau)$ and p(x), respectively. By taking an ensemble average over all the possible
321 realizations of the unresolved heterogeneity, it is possible to map the set of small-scale,
322 unresolved heterogeneities onto a probabilistic distribution of retention times, $\psi(\tau)$, that
323 contains all the information necessary to describe transport in a given heterogeneous
324 media. The p(x) pdf is assumed to have finite variance; from a physical point of view,
325 this means that the tracer is allowed to take only relatively short jumps—consistent with
326 the geological picture we have of a fractured porous matrix.
327
328 A comprehensive discussion of the CTRW and its relation to other upscaling methods can be found in the
329 recent review by Berkowitz et al. (2006). We refer to this review for the theoretical development of the
330 CTRW, while details regarding the numerical implementation can be found in Cortis and Berkowitz
331 (2005). In this work, we use, as the starting point of our analysis, the CTRW partial differential equation
332 (PDE) for the transport of a passive tracer. In its nondimensional form, the CTRW PDE that governs the
333 spatio-temporal evolution of the density of a passive tracer, c(x,τ), is (Dentz et al., 2004):

334 $$u\tilde{c}(x,u) - c_0(x) = -\tilde{M}(u)\partial_x\left[\tilde{c}(x,u) - \alpha\partial_x\tilde{c}(x,u)\right] \qquad (1)$$

335

336 where the tilde indicates the Laplace transform (LT) $\tilde{f}(u) = L[f(\tau)] = \int_0^\infty f(\tau)\exp(-u\tau)d\tau$,

337 u is the Laplace variable, $c_0(x)$ is the initial condition, α is the local dispersivity, and

338 $\tilde{M}(u)$ is a memory function that takes into account the nature of the heterogeneity and is

339 related to the retention times pdf, $\psi(u)$, by $\tilde{M}(u) = u\dfrac{\tilde{\psi}(u)}{1-\tilde{\psi}(u)}$. In Equation (1), length

340 and times have been made nondimensional, such that the nondimensional transport
341 velocity is equal to unity. Equation (1) represents the time convolution of the memory

342 function M(τ) with the classical advection-dispersion operator, and for this reason this
343 class of models is referred to as nonlocal in time. Equation (1) reduces to the classical
344 ADE when $\tilde{M}(u)=1$; i.e., M(τ)=δ(τ), which implies an exponentially fast decay of the
345 retention times pdf, $\tilde{\psi}(u)=\frac{1}{1+u}$, i.e., ψ(τ)=exp(−τ). It can also be shown that fractional
346 derivative models are special cases of the general CTRW formulation (Berkowitz et al.,
347 2006).
348
349 The CTRW interpretation of the dispersivity α is different from the classical advection-
350 dispersion equation (ADE). In the ADE, α represents a typical characteristic length of the
351 small features of the systems, e.g., the pore-throat size. This interpretation has been a
352 problematic one from its inception, and has led to a vast literature on the so-called
353 macroscopic dispersion tensor, i.e., the attempt of explaining the scale-dependent
354 spreading of observed tracer BTCs by means of an evolving characteristic length. Instead,
355 in the CTRW approach, α is defined as the ratio

356 $$\alpha=\frac{1}{2}\frac{\int p(x)x^2\mathrm{d}x}{\int p(x)x\mathrm{d}x}. \qquad (2)$$

357
358 The ψ(τ) pdf completely describes, in a probabilistic sense, the entire range of
359 interactions that a solute molecule experiences in its interactions with the fluid flow field.
360 Heterogeneities in the flow field have a strong influence on the retention-time probability
361 of staying in a given place for a given interval of time, as is the case for high retention
362 times in stagnation zones (such as those in low-permeability matrix blocks) and short

363 retention times for fast flow paths (such as those in interconnected fractures). In other
364 words, the CTRW approach smoothes out the unresolved heterogeneities and maps them
365 onto the $\psi(\tau)$ retention times pdf. This mapping has the effect of representing the overall
366 effect of the heterogeneities through a time-memory convolution, which reflects the
367 history of interactions within the system.
368
369 As discussed in Dentz et al., (2004), an algebraically decaying $\psi(t) \sim \tau^{-1-\beta}$ can explain a
370 power-law like type of decay for the tail of a breakthrough curve. This type of long
371 tailing is illustrated in Figure 5, where we plotted the solution of the ADE equation for a
372 dimensionless velocity of v=1 and a dimensionless dispersivity α=0.005 (solid blue line),
373 and the CTRW solution corresponding to the $\tilde{\psi}(u) = \frac{1}{1+u^{\beta}}$, with β=0.8, and α=0.005
374 (solid red line). We recall that the ADE solution corresponds to $\tilde{\psi}(u) = \frac{1}{1+u}$. The long
375 tailing in the CTRW solution is caused by the convolution of the memory function with
376 the ADE transport operator (solid blue line). We note that the explicit solution of the
377 CTRW equation is more than just a simple convolution of the memory function
378 $\tilde{M}(u)$ with the solution for the ADE equation (see ,e.g., the Appendix B of Dentz et al.,
379 2004,). Depending on the specific shape of $\psi(\tau)$, the CTRW model can reproduce the fast
380 early-time arrivals as well as the long tailing typical of fractured systems, as illustrated in
381 Figure 5.
382
383 Typically, the CTRW PDE is solved by postulating a simple functional form for $\psi(\tau)$ and
384 then fitting its model parameters to the experimental data. A number of $\psi(\tau)$ models are

385 described in detail in Berkowitz et al. (2006). Despite the wide success in fitting many
386 laboratory and field datasets, however, such simple functional forms may not be general
387 enough to describe the entire range of transport modes encountered in hydrogeological
388 applications (Anwar et al., 2007). Following this approach, we have tried to fit the BTCs
389 in Figure 4 with all the functional forms described in Berkowitz et al. (2006), with no
390 success. Attempts to generalize these functional forms to conform to the shape of these
391 BTCs also failed. Thus, a more general and less restrictive method needs to be used in
392 this case. For this reason, in this work we apply a nonparametric inversion algorithm
393 (NPIA) first described in Cortis (2007).
394
395 The NPIA is aimed at recovering the numerical approximation of the whole spectrum of
396 retention times that govern transport directly from the experimental data, without
397 postulating *a priori* a functional form for $\psi(\tau)$. While the details of the NPIA can be
398 found in Cortis (2007), below we summarize the salient features of the method. In the
399 NPIA, the $\psi(\tau)$ is given through its numerical representation in the time-interval interest
400 depending on the evolution of the breakthrough. This representation is obtained through
401 the numerical inversion of the numerical approximation of $\tilde{\psi}(u)$, determined via a
402 nonlinear numerical inversion of the best fit of the CTRW PDE solution to the numerical
403 Laplace-transformed data. The method is robust enough to reproduce all the known
404 functional forms for $\psi(\tau)$, and yet flexible enough to represent more complex-looking
405 BTCs. One of the most notable results of the application of the nonparametric approach
406 to nonlocal methods is that any given unresolved heterogeneity can be represented by a
407 family of retention-time probability distributions, $\psi(\tau|\alpha)$ of parameter α, where α is the

local dispersivity. In other words, any given set of breakthrough curves taken at different sections, and/or concentration profiles taken at different times, can be fit equally well by different $\psi(\tau)$, conditional to some reasonable value of α. This means that the dispersivity α cannot be considered either an intrinsic or a scale-dependent parameter of the system. Importantly, as no *a priori* value of α can be given or estimated from any type of macroscopic measurement, it must be interpreted only as an ancillary parameter of the retention-time probability distribution $\psi(\tau)$, which fully describes the transport. These considerations hold true not only for systems exhibiting anomalous transport, but also for normal transport, i.e., for the classical ADE Gaussian type of transport (Cortis, 2007).

3.3 Application of the CTRW Method

The first step in applying the CTRW model to the BTCs (shown in Figure 4) is the definition of characteristic (dimensional) transport velocity v' and dispersivity α' for the different fracture-matrix systems studied in Section 2.

As discussed earlier, in our CTRW model, the interaction between the fractures and the porous matrix is fully taken into account via the introduction of the memory function $M(\tau)$ (hence the probabilistic distribution of retention times, $\psi(\tau)$), which is convoluted with the classical ADE transport kernel, i.e., $v'\partial_x\left[c(x,t)-\alpha'\partial_x c(x,t)\right]$. We thus need to define reasonable values for the relevant parameters v' and α' of the classical ADE that represent the local dispersion inside the porous matrix and along single fractures, without accounting for their interaction.

One logical approach is to define the characteristic transport velocity of the composite system in Figure 2 using the total flux through the fracture-matrix column (to calculate the Darcy velocity) and the total porosity of the fractured porous medium (to convert from Darcy to transport velocity). In other words, we calculate the velocity v' that represents a homogeneous column conducting the same total flux and has the same pore space as the fracture-matrix systems studied in Cases 1 through 4. Note that both these quantities—total flux and porosity—can generally be measured or estimated in field situations. Similarly, the dispersivity α' can be chosen such that it represents only local dispersive effects in fractures and matrix blocks, and not the effects stemming from the fracture-matrix interaction. The exact value of α' is not important because, as discussed above, the application of the nonparametric inversion algorithm implies that equally good fits of the CTRW equations on the BTCs data can be obtained for different (reasonable) values of the dispersivity (Cortis, 2007). In this work, we selected a value of α'=0.25 m, that, as we will see in the discussion below, represent the characteristic dispersivity of Case 4. Such value of α' is considerably smaller than the typical macrodispersivity estimates (Gelhar, 1993).

We define dimensionless parameters as follows. Length-based quantities such as horizontal distance or dispersivity are normalized with the total length of the model domain, L=50 m. The four BTC locations shown in Figure 4, at 2, 10, 30, and 90 sectors (1, 5, 15, 45 m), thus correspond to nondimensional distances of x=[0.02, 0.1, 0.3, 0.9]. Nondimensional dispersivity is α=0.005. The characteristic transport velocity calculated

454 above is normalized to unity, and time in the breakthrough curves is normalized such that
455 a particle migrating with unit velocity would arrive at the end of the column, x=1, at
456 nondimensional time τ=1. We then select the BTC calculated at x=0.1 as the reference
457 BTC for the CTRW model: this will be our "data." In other words, the breakthrough
458 results from the discrete simulations for the cross section at 10 sectors (Figure 4)
459 represent the data set over which the nonparametric inversion algorithm is fitted to. The
460 NPIA yields the $\psi(\tau|\alpha)$ retention time pdf, conditional to the chosen value of α. The
461 $\psi(\tau|\alpha)$ is then used to predict the BTCs at x=0.02, x=0.3, and x=0.9. This procedure is
462 conducted for all parameter cases, by keeping the value of α unchanged.
463
464 We recall that Case 1 represents the one bounding case in which a very small flux is
465 allowed to flow in the porous matrix (low permeability). Cases 2, 3, and 4 have
466 increasing matrix-permeability values, with Case 4 the other bounding case, in which an
467 equal amount of flux is allowed in the fractures and the porous matrix.
468
469 The results of the fitting procedure to Cases 1 through 4 are reported in Figure 6. In the
470 left panels of Figure 6, we plotted as solid lines the simulated BTCs at the four sections
471 x=[0.02, 0.1, 0.3, 0.9] (as calculated by the discrete numerical procedure), together with
472 the best fits obtained by means of our NPIA applied to the CTRW model (circles). The
473 ADE model α = 0.005 is also reported for reference (dashed lines). In the right panel of
474 Figure 6, we plotted, in double logarithmic units as a solid line, the best fit $\psi(\tau)$ obtained
475 with the NPIA on the BTC at x=0.1 and as a reference the exponential function $\exp(-\tau)$,
476 which represents the ADE model limit.

As we can see from Figure (6), the ADE model does a good job at fitting the BTCs in Case 4 (for x=0.1) and predicting the BTC at the other sections. This can be seen also from the best fit $\psi(\tau)$ (solid line), which is very close to the decaying exponential $\exp(-\tau)$ (dashed line), i.e., the ADE limit. In other words, the observed "correct" BTC of the fracture-matrix system can be represented without explicitly accounting for unresolved heterogeneities. This is not too surprising, considering the strong mixing between fracture and matrix flow (Figure 3) and the typical symmetrical shape of the breakthrough curve (Figure 4). In this case, however, the CTRW model is slightly more precise than the ADE. Notice that the good agreement between the "correct" BTC and the ADE solution also supports the determination of the characteristic transport velocity of the composite system.

As the total flux in the system predominantly flows in the fractures for the cases with small matrix permeability (Cases 1 through 3), the ADE fails in predicting the BTCs, whereas the CTRW model provides excellent fits (for x=0.1) and predictions (for x=[0.02, 0.3, 0.9]). (For the section at x=0.02, the CTRW model provides a correct prediction only up to the time at which the reference BTC used to derive the $\psi(\tau)$ pdf (in our examples the BTC at x=0.1) differs significantly from zero. In other words, because of the inherent numerical instability of the numerical Laplace inversion algorithms (i.e., the oscillating behavior), the numerical approximation of $\psi(\tau)$ is not accurate enough to back-propagate the BTC for small enough times.) The CTRW approach is capable of representing transport processes for a wide range of fractured porous formations, ranging

500 from mobile-immobile systems with mostly diffusive mixing (Figure 3(a) for Case 1) to
501 mobile-mobile systems with diffusive as well as advective-dispersive mixing (Figures
502 3(b) and 3(c) for Cases 2 and 3).
503
504 In each of these three cases, the best-fit $\psi(\tau)$ pdfs consistently deviate from the decaying
505 exponential, which indicates the presence of a wider spectrum of characteristic retention
506 times in the fracture-matrix system. We can observe the graph of the best-fit $\psi(\tau)$ (solid
507 line) crossing the graph of the decaying exponential (dashed line). Retention times larger
508 than $\exp(-\tau)$ are indications of faster tracer arrivals, whereas smaller values indicate
509 slower tracer arrivals. This behavior can be understood by recalling the characteristics of
510 the fracture-matrix interaction as shown in Figure 3. We also note that the best-fit $\psi(\tau)$
511 converges, for long times, to a decaying exponential behavior, a clear indication of a
512 truncation time for the transport process (Dentz et al, 2004). Consistent with this
513 observation, the crossing time decreases with the increase of the matrix permeability.
514
515 It is also worth pointing out that the estimated $\psi(\tau)$ pdfs show a $\tau^{-1/2}$ slope for Cases 1
516 through 3, which is often observed in field conditions and interpreted as macroscopic
517 matrix diffusion. While Cases 1 and 2 are definitely diffusion dominated in the matrix,
518 Case 3 exhibits clearly the effect of advective transport through the matrix blocks. It
519 appears that diffusive and advective interaction between fractures and matrix lead to the
520 same slope in the estimated $\psi(\tau)$ pdfs. This suggests that the macroscopic values of
521 matrix diffusion determined in field conditions, which are often larger than those
522 observed in laboratory conditions, may include contributions stemming from advective

transport in the porous matrix. A interesting topic of research would be a study of the relationship between the transition cut-off time from a $\tau^{-1/2}$ slope to a decaying exponential behavior in the $\psi(\tau)$, and its dependence on the permeability characteristics of the fractures and the matrix.

Note that the value for dispersivity α remains unchanged for the four cases, so that the transport is completely defined by the $\psi(\tau|\alpha)$ pdf. Furthermore, within each individual case, a single value of α is used to describe the BTCs for the four locations, whereas a macrodispersivity approach would require a scale-dependent and much larger value of $\alpha = \alpha(x)$. Our sensitivity study indicates that the quality of the CTRW fitting results does not depend on the particular (small) value of α, in accordance with the results of Cortis (2007) describing the existence of a family of residence time pdfs parameterized in α. This confirms our initial conjecture that small values of α can be thought of as accounting for the small local dispersion and diffusion phenomena happening in the individual fractures and matrix blocks, whereas the fracture-matrix interaction can be represented by a memory function related to the tracer retention-times probabilistic distribution.

4. Conclusions

We have presented a study of the tracer-transport interaction in a composite hydrogeological system consisting of interconnected fractures and porous permeable matrix blocks. Four sensitivity cases, covering a wide range of matrix permeability values, exhibited a macroscopic transport behavior strongly dependent on the intrinsic heterogeneity of the fractured rock (i.e., fractures versus matrix) and the characteristics of local fracture-matrix interaction processes. Using results from numerical experiments employing a discrete (microscopic) representation of fractures and matrix, we investigated the possibility of the Continuous Time Random Walk (CTRW) framework for predicting the observed macroscopic transport processes in such composite media.

Our results indicate that:

1. The CTRW offers a valid and robust alternative to classical approaches used for fractured porous media (such as dual-continuum models), with a clear physical interpretation and a parsimonious number of parameters;
2. The anomalous transport observed in the numerical experiments can be fully characterized by the probabilistic distribution function (pdf) of retention times, $\psi(\tau)$, which stochastically describes the full range of interactions between the fractures and porous matrix;
3. The $\psi(\tau)$ pdf can be extracted by means of a nonparametric inversion algorithm fitted on the observed breakthrough data at a given location, which fully characterizes the transport at all other locations;

4. The characteristic transport velocity used in the CTRW approach can be calculated from the total composite flux and the total composite porosity of the fractured formation;
5. The dispersivity α used in the CTRW is not scale-dependent, such that one value of α can be used for all sensitivity cases and locations. Moreover, the relatively small value used for α represents the local dispersion in single fractures or matrix blocks, but does not need to account for the complex interaction between fractures and matrix that leads to the anomalous macroscopic behavior. As discussed above, the latter is fully characterized by the pdf of retention times;
6. Anomalous early-time arrivals can also be represented in the CTRW framework, and are characterized by values of $\psi(\tau) > \exp(-\tau)$ for times smaller than some crossover value τ', whereas the slow late-time arrivals are characterized by values of $\psi(\tau) < \exp(-\tau)$.

Future work will focus on CTRW applications to more disordered fracture-matrix systems, looking at the effects of random fracture structures or evaluating the impact of microscopic heterogeneities within the fractures or the porous matrix, hence requiring a local $\psi(\tau)$ for these local structures. We will also attempt to apply the CTRW methods developed here to field data from fractured porous media.

Acknowledgments

This work was supported by the U.S. Department of Energy under contract No. **DE-AC02-05CH11231**. Review and comments of T.A. Ghezzehei (LBNL) are greatly appreciated.

References

Ahmadi, A., Quintard, M., Whitaker, S. (1998), Transport in Chemically and Mechanically Heterogeneous Porous Media V. Two-Equation Model for Solute Transport with Adsorption, Advances in Water Resources, 22(1), pp. 59-86.

Anwar, S., Cortis, A., and Sukop, M.C. (2007) Lattice Boltzmann Simulation of Solute Transport in Heterogeneous Porous Media with Conduits to Estimate Macroscopic Continuous Time Random Walk Model Parameters. Progress in Computational Fluid Dynamics(in press).

Barenblatt, G.E., Zheltov, I.P., Kochina, I.N. (1960), Basic Concept on the Theory of Homogeneous Liquids in Fissured Rocks, J. Appl. Math. Mech., Engl. Transl., 20, pp. 852-864.

Berkowitz, B., Bear, J., Braester, C. (1988), Continuum Models for Contaminant Transport in Fractured Porous Formations", Water Resources Research, 24(8), pp. 1225-1236.

Berkowitz, B. (2002), Characterizing Flow and Transport in Fractured Geological Media: A Review, Advances in Water Resources, 25, pp. 861-884.

Berkowitz, B., Cortis, A., Dentz, M., Scher, H. (2006), Modeling Non-Fickian Transport in Geological Formations Rev. Geophys., Reviews of Geophysics, 44 (2): Art. No. RG2003

Bibby, R. (1981), Mass Transport of Solutes in Dual-Porosity Media, Water Resources Research, 17(4), pp. 1075-1081.

612 Birkholzer, J., Rubin, H., Daniels, H., Rouve, G. (1993a): Contaminant Advection and
613 Spreading in a Fractured Permeable Formation: Part 1. Parametric Evaluation and
614 Analytical Solution, Journal of Hydrology, 144, pp. 1-33.

615 Birkholzer, J., Rubin, H., Daniels, H., Rouve, G. (1993b): Contaminant Advection and
616 Spreading in a Fractured Permeable Formation: Part 2. Numerical Simulation, Journal
617 of Hydrology, 144, pp. 35-58.

618 Birkholzer, J., Rouve, G. (1994): Dual-Continuum Modeling of Contaminant Transport
619 in Fractured Formations, Proceedings X International Conference on Computational
620 Methods in Water Resources, Heidelberg, Germany.

621 Boano, F., Packman, A.I., Cortis, A. Revelli, R., Ridolfi, L. (2007), A continuous time
622 random walk approach to the stream transport of solutes, Water Resources Research,
623 doi:10.1029/2007WR006062, in press.

624 Bijeljic, B., Blunt, M. (2006), Pore-scale modeling and continuous time random walk
625 analysis of dispersion in porous media, Water Resources Research, Vol. 42(1): 5. doi:
626 10.1029/2005WR004578. issn: 0043-1397.

627 Bodin, J., Delay, F., de Marsily, G. (2004), Solute transport in a single fracture with
628 negligible matrix permeability. 2. Mathematical formalism, Hydrogeology Journal
629 Vol. 11, pp. 434-454.

630 Cherblanc, F., Ahmadi, A., Quintard, M. (2003), Two-Domain description of Dispersion
631 in Heterogeneous Porous Media: Calculation of Macroscopic Properties, Water
632 Resources Research, 39(6), pp. 1154ff.

633 Cherblanc, F., Ahmadi, A., Quintard, M. (2007), Two-Domain Description of Solute
634 Transport in Heterogeneous Porous Media: Comparison Between Theoretical

635 Predictions and Numerical Experiments, Advances in Water Resources, 30, pp. 1127-
636 1143.

637 Cortis, A. (2007), Péclet-dependent memory kernels for transport in heterogeneous media,
638 Phys. Rev. E 76, 030102(R).

639 Cortis, A. and Ghezzehei T.A. (2007), On the transport of emulsions in porous media, J.
640 Colloid and Interface Science 313 (1): 1-4.

641 Cortis, A. and Knudby C. (2006), A CTRW approach To Anomalous Transient Flow in
642 Heterogeneous Porous Media, Water Resour. Res., 42 (10): Art. No. W10201.

643 Cortis, A., Harter, T., Hou, L., Atwill, E. R., Packman, A., Green, P. (2006), Long-time
644 Elution of Cryptosporidium Parvum Oocysts in Porous Media Water Resour. Res., 42
645 (12): Art. No. W12S13.

646 Cortis A. and Berkowitz B. (2005), Computing ‘‘Anomalous’’ Contaminant Transport in
647 Porous Media: The CTRW MATLAB Toolbox, Ground Water Vol. 43, No. 6,
648 November–December 2005, 947–950.

649 Cortis, A., Chen, Y., Scher, H., Berkowitz, B. (2004), Quantitative characterization of
650 porescale disorder on transport in “homogeneous” granular media. Phys. Rev. E,
651 70(4):041108.

652 Cortis, A. and Berkowitz, B. (2004), Anomalous transport in “classical” soil and sand
653 columns, Soil Sci. Soc. Am. J., 68: 1539-1548.

654 Dentz, M., Berkowitz, B. (2003), Transport Behavior of a Passive Solute in Continuous
655 Time Random Walks and Multirate Mass Transfer, Water Resources Research, 39(5),
656 pp. 1111ff.

657 Dentz, M., Cortis, A., Scher, H., and Berkowitz, B. (2004). Time behavior of solute
658 transport in heterogeneous media: transition from anomalous to normal transport.
659 Adv. Water Resour., 27(2):155–173, doi:10.1016/j.advwatres.2003.11.002

660 Dykhuizen, R.C. (1990), A New Coupling Term for Dual-Porosity Models, Water
661 Resources Research, Vol. 26, No. 2, pp. 351-356.

662 Feehley, C.E., Zheng, C., Molz, F.J. (2000), A Dual-Domain Mass transfer Approach for
663 Modeling Solute Transport in Heterogeneous Aquifers: Application to the
664 Macrodispersion Experiment (MADE) Site, Water Resources Research, 36(9), pp.
665 2501-2515.

666 Flach, G.P., Crisman, S.A., Molz, F.J. (2004), Comparison Between Single-Domain and
667 Dual-Domain Subsurface Transport Models, Groundwater, 42(6), pp. 815-828.

668 Gerke, H.H., van Genuchten, M.T. (1993a), A Dual-Porosity Model for Simulating the
669 Preferential Movement of Water and Solutes in Structured Porous Media, Water
670 Resources Research, 29(2), 305-319.

671 Gerke, H.H., van Genuchten, M.T. (1993b), Evaluation of a First-Order Water Transfer
672 Term for Variably Saturated Dual-Porosity Flow Models, Water Resources Research,
673 Vol. 29(4), pp. 1225-1238.

674 Gwo, J-P., O'Brien, R., Jardine, P.M. (1998), Mass Transfer in Structured Porous Media:
675 Embedding Mesoscale Structure and Microscale Hydrodynamics in a Two-Region
676 Model, Journal of Hydrology, 208, pp. 204-222.

677 Haggerty, R., Gorelick, S.M. (1995), Multiple-Rate Mass Transfer for Modeling
678 Diffusion and Surface reactions in Media with Pore-Scale Heterogeneity, Water
679 Resources Research, 31(10), pp. 2383-2400.

680 Huyakorn, P.S., Lester, B.H., Faust, C.R. (1983a), Finite Element Techniques for
681 Modeling Groundwater Flow in Fractured Aquifers, Water Resources Research, 19(4),
682 pp. 1019-1035.

683 Huyakorn, P.S., Lester, B.H., Mercer, J.W. (1983b), An Efficient Finite Element
684 Technique for Modeling Transport in Fractured Porous Media: 1. Single Species
685 Transport, Water Resources Research, Vol. 19(3), pp. 841-854.

686 Huyakorn, P.S., Lester, B.H., Mercer, J.W. (1983c), An Efficient Finite Element
687 Technique for Modeling Transport in Fractured Porous Media: 2. Nuclide Decay
688 Chain Transport, Water Resources Research, Vol. 19(5), pp. 1286-1296.

689 Lagendijk, V.R. (2005), Stofftransportvorgänge in Festgesteinsaquiferen: Analyse von
690 Tracerdurchbruchskurven zur Identifikation eines geeigneten Mehrkontinuum-
691 Ansatzes, Ph.-D. Thesis, Proceedings 140, IWW, Aachen University of Technology.

692 Landereau P., Noetinger B., Quintard M., (2001), Quasi steady two equation models for
693 transport in fractured porous media: Large scale properties for densely fractured
694 systems, Advances in Water Resources, Vol. 24(8), pp. 863-876.

695 Neuman, S.P. (2005), Trends, Prospects and Challenges in Quantifying Flow and
696 Transport Through Fractured Rocks, Hydrogeology Journal, 13, 124-147.

697 Noetinger B., Estebenet T., and Landereau P., (2001), A direct determination of the
698 transient exchange term of fractured media using a continuous time random walk
699 method, Transport in Porous Media, Vol. 44, pp. 539-557.

700 Noetinger B., Estebenet T., and Quintard M., (2001), Up scaling flow in fractured media:
701 equivalence between the large scale averaging theory and the continuous time random
702 walk method, Transport in Porous Media, Vol. 43, pp. 581-596.

703 Roth, K., Jury, W.A. (1993): Linear Transport Models for Adsorbing Solutes, Water
704 Resources Research, Vol. 29(4), pp. 1195-1204.
705 Rubin, H., Soliman, A.M., Birkholzer, J., Rouve, G. (1996): Transport of a Tracer Slug in
706 a Fractured Permeable Formation, Journal of Hydrology, 176, pp. 153-180.
707 Simunek J., Jarvis, N.J., Van Genuchten, M.T., Gaerdenaes, A. (2003), Review and
708 Comparison of Models for describing Non-Equilibrium and Preferential Flow and
709 Transport in the Vadose Zone, Journal of Hydrology, 272, pp. 14-35.
710 Teutsch, G. (1990), An Extended Double-Porosity Concept as a Practical Modeling
711 Approach for Karstified Terranes, Int. Symp. Field Seminar on Hydrogeological
712 Processes in Karst Terranes, 7. - 17. Oct. 1990, Antalya, Turkey.
713 Zimmerman, R.W., Chen, G., Hadgu, T., Bodvarsson, G.S. (1993), A Numerical Dual-
714 Porosity Model with Semianalytical Treatment of Fracture/Matrix Flow, Water
715 Resources Research, Vol. 29(7), pp. 2127-2137.
716 Zimmerman, R.W., Bodvarsson, G.S., Kwicklis, E.M. (1990), Adsorption of Water into
717 Porous Blocks of Various Shapes and Sizes, Water Resources Research, Vol. 26(11), pp.
718 2797-2806.

719 Table 1: Geometry and properties chosen for discrete simulation

Parameter	Value	Unit
Fractures		
Fracture Spacing, B	0.707	m
Angle Between Fractures and x – Direction, θ	45	°
Aperture, a	10^{-4}	m
Hydraulic Conductivity of Single Fracture[1]**,** K_s^F	703	m/d
Continuum Conductivity in x – Direction[2]**,** K^F	9.94×10^{-2}	m/d
Equivalent Continuum Porosity[3]**,** n^F	2.83×10^{-4}	-
Longitudinal Dispersivity Along Single Fracture, α_l^F	0.01	m
Effective Diffusion in Single Fracture Coefficient, D_{mo}^F	10^{-4}	m^2/d
Matrix[4]		
Porosity, n^M	0.05	-
Hydraulic Conductivity, K^M	case dependent	m/d
Longitudinal Dispersivity, α_l^M	0.01	m
Transverse Dispersivity, α_t^M	0.001	m
Effective Diffusion Coefficient[5]**,** D_{mo}^M	2.0×10^{-5}	m^2/d
Size of Matrix Blocks, $B \times B$	0.707×0.707	m^2
Other		
Hydraulic Gradient in x - Direction, J	0.01	-
Sector Length, L	0.5	m

720 [1] Calculated from parallel plate assumption as follows: $K_s^F = g(2b)^2 / 12\nu$

721 [2] Calculated from geometry considerations as follows: $K^F = K_s^F \cos\theta / (B \sin\theta)$

722 [3] Calculated from geometry considerations as follows: $n^F = a / (B \sin\theta \cos\theta)$

723 [4] Properties are given for unit bulk volume of the rock matrix

724 [5] Includes effect of tortuosity, assumed to be 0.2

725

726

726 Table 2: Sensitivity Cases

	Case 1	Case 2	Case 3	Case 4
Formation Type	e.g., crystalline rock, shale	e.g., porous sandstone, limestone		
Matrix Hydraulic Conductivity	8.3×10^{-6} m/d	2×10^{-3} m/d	8.3×10^{-3} m/d	9.94×10^{-2} m/d
Ratio Fracture to Matrix Continuum Conductivity	≈ 12,000	50	12	1
Ratio Fracture to Matrix Transport Velocity[1]	$\approx 3 \times 10^{6}$ m/d	≈ 12,400	≈ 3,000	250
Type of Fracture-Matrix Interaction[2]	Almost Purely Diffusive	Mostly Diffusion	Diffusion and Advection	Mostly Advection, Strong Mixing
Breakthrough Characteristics[2]	Rapid Response, Long Tail	Between Cases 1 and 4		Typical ADE[3] without tailing

727 [1] Fracture transport velocity is measured along fracture axis.

728 [2] Based on Birkholzer & Rouve (1994)

729 [3] ADE: Advection-Dispersion Equation

730

731

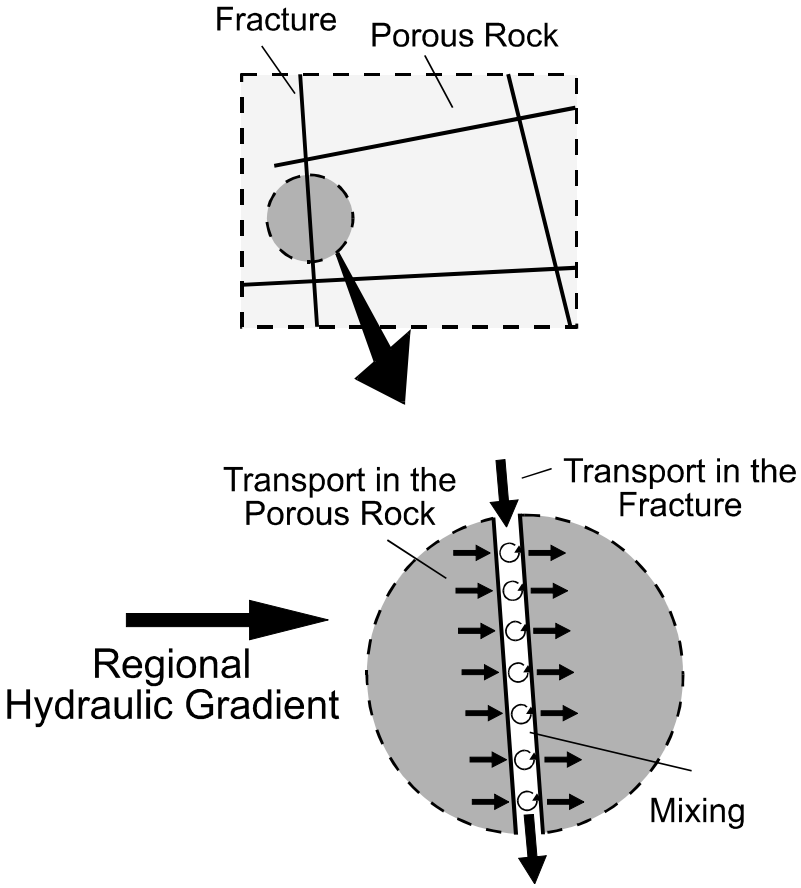

731

732

733 Figure 1: Schematic showing the mixing between fracture and matrix flow as a result of

734 convective transport in the matrix

735

736

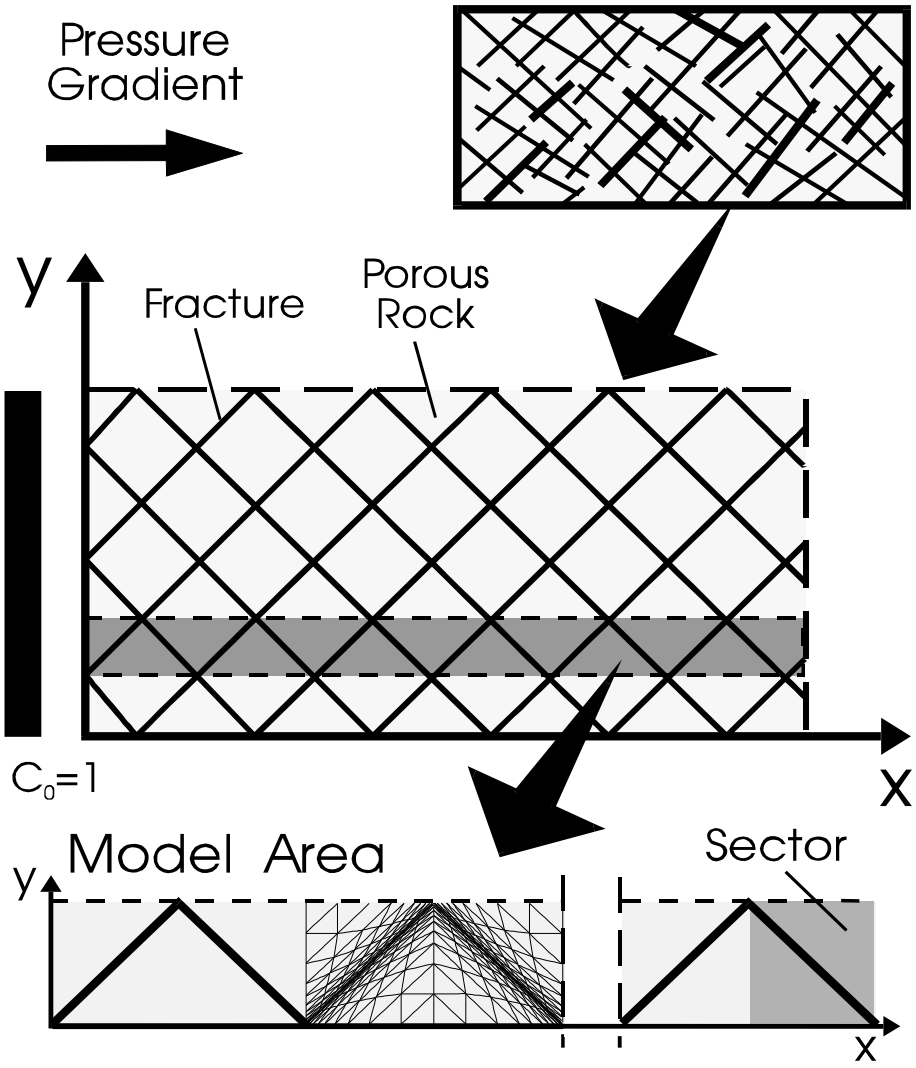

Figure 2. Discrete representation in idealized fracture network. Flow and transport is from left to right, with a concentration boundary condition on the left side. The total domain is 100 sectors long.

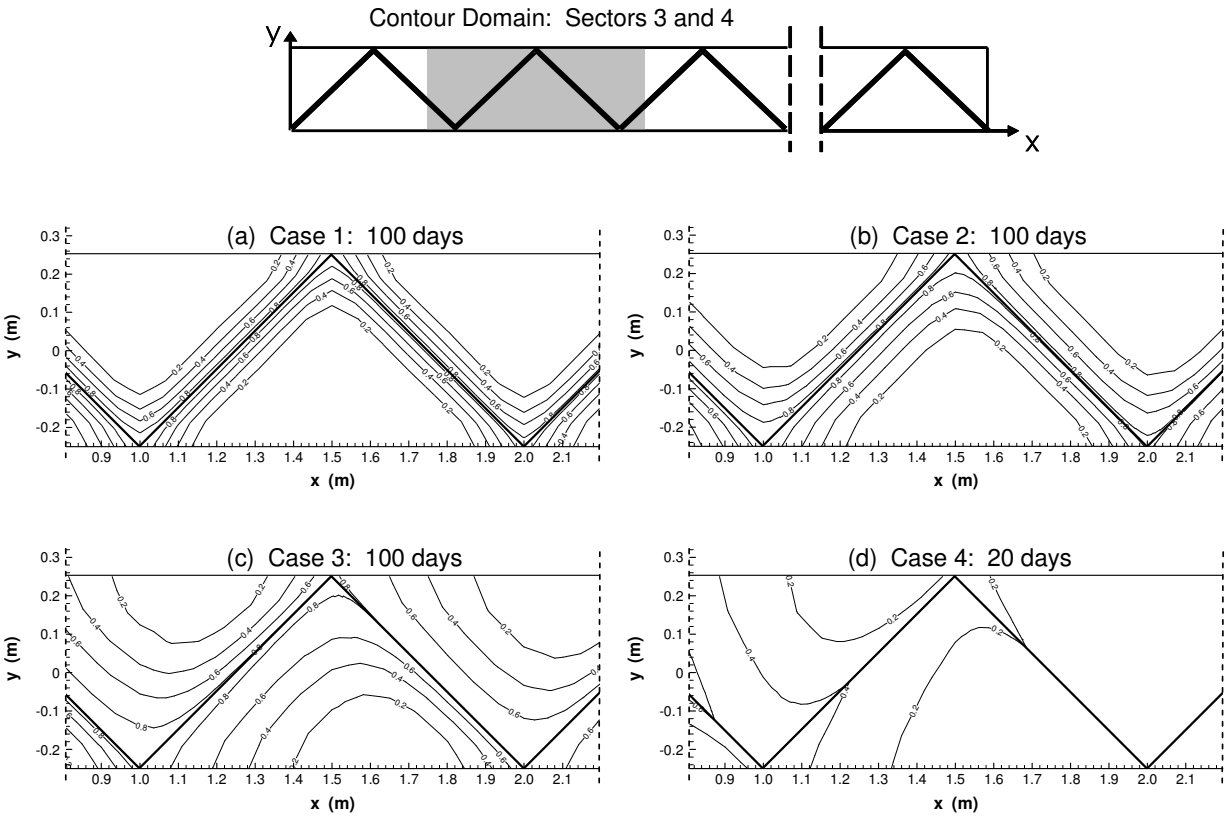

741

742 Figure 3. Matrix concentrations from discrete simulations displayed in sectors 3 and 4 of

743 the model domain.

744

744

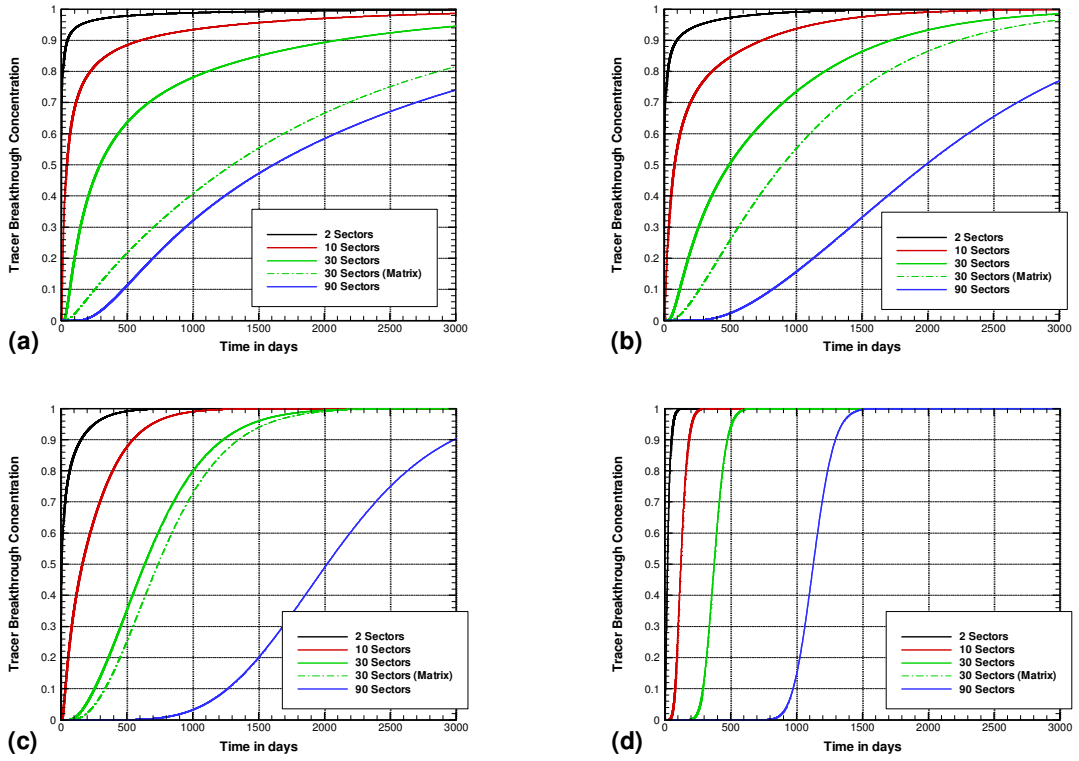

745

746 Figure 4. Breakthrough curves for (a) Case 1, (b) Case 2, (c) Case 3, and (d) Case 4,

747 measured at different locations along the model domain.

748

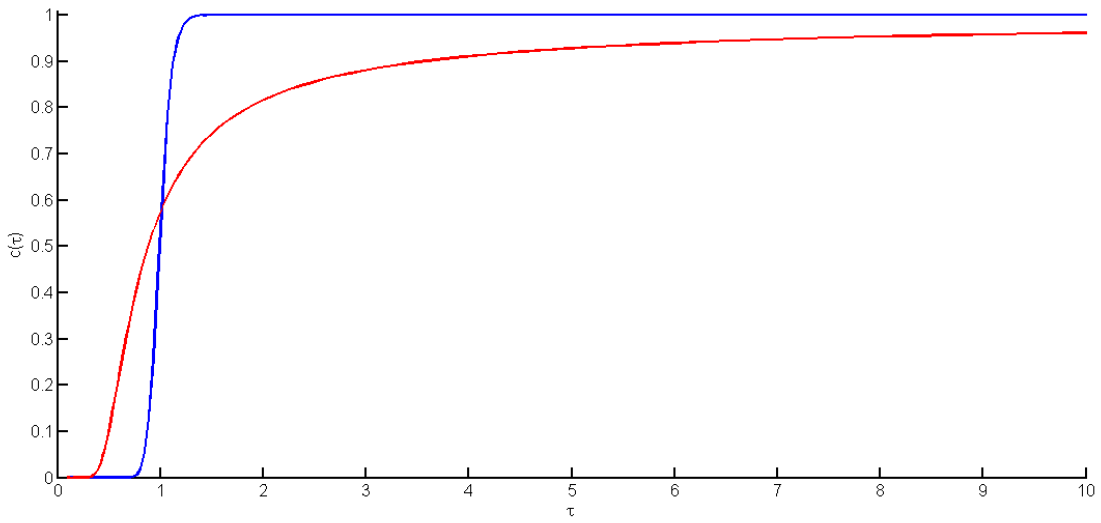

748

749 Figure 5. ADE solution (solid blue line) and CTRW solution (solid red line), for the

750 same value of the non-dimensional dispersivity α=0.005. For the CTRW

751 solution, $\tilde{\psi}(u) = \frac{1}{1+u^{\beta}}$, with β=0.8.

752

753

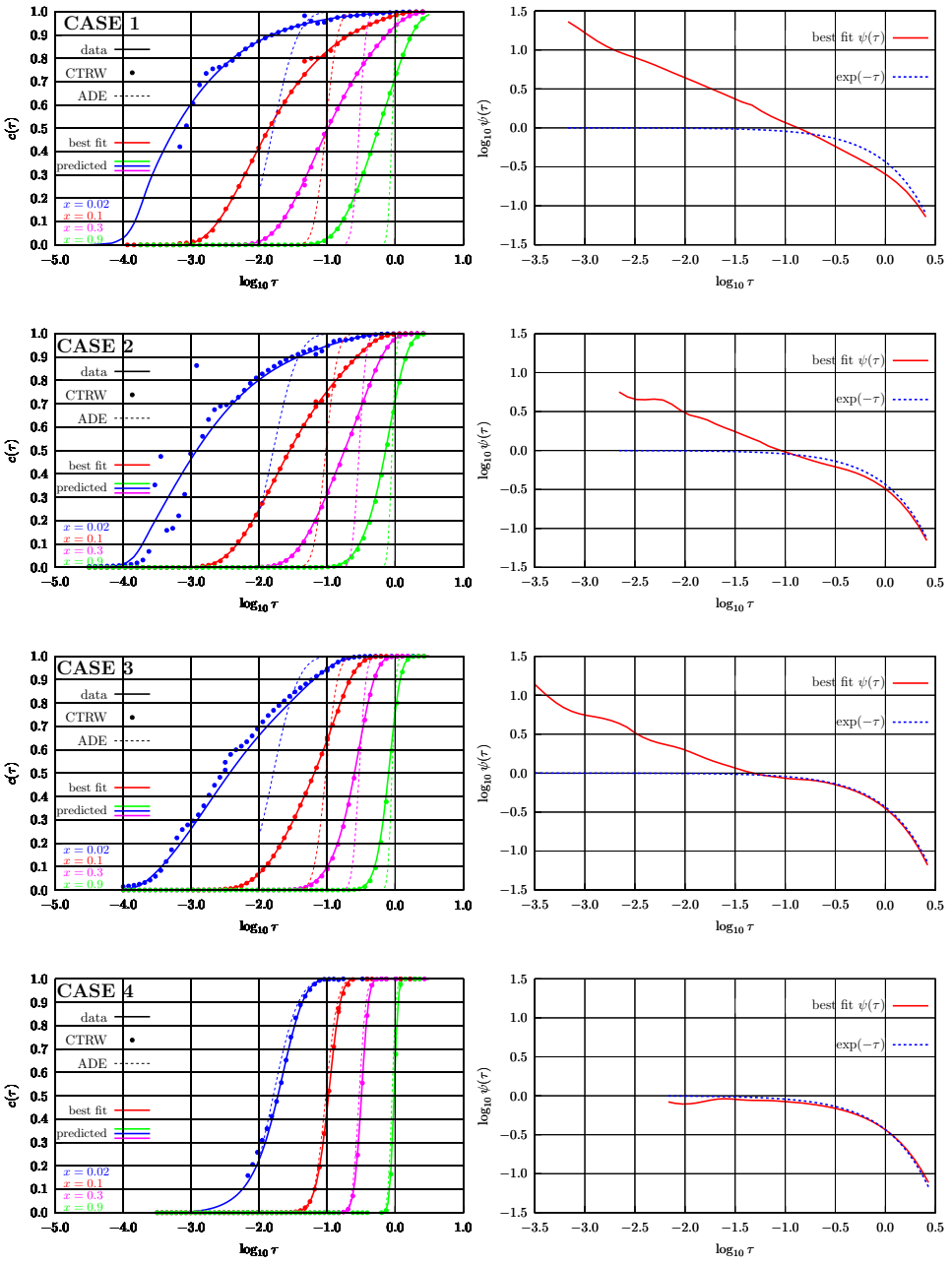

Figure 6: Best fit results of the CTRW model. Cases 1-4, (top to bottom) represent systems with increasing values of the porous matrix (See Table 2). In the left panel we compare the discrete numerical computations (solid lines), with the CTRW model (circles) and the ADE model (dashed lines). The breakthrough curves are calculated at four different sections, x=0.02, 0.1, 0.3, and 0.9. In the right panel, we plot the best fit probabilistic distribution of retention times, ψ(τ) (solid lines), and for comparison the decaying exponential exp(-τ) (dashed lines), the classical ADE limit.